

Article

Geochronology and Tectonic Implications of the Nianzigou Granites and Associated Mo Deposit, Inner Mongolia

Yang Li ^{1,*}, Yongqiang Yang ^{1,*}, Lei Hua ¹, Yaxing Leng ²  and Jiang Xin ³

¹ State Key Laboratory of Geological Processes and Mineral Resources, China University of Geosciences, Beijing 100083, China; dxqy8@cugb.edu.cn

² Institute of Geology, CAGS, Beijing 100037, China; yaxing.leng@gmail.com

³ West Gold Ltd., Co., Urumqi 830002, China; xinjiang_111@163.com

* Correspondence: liy001@cugb.edu.cn (Y.L.); yangyongq@cugb.edu.cn (Y.Y.)

Abstract: Multiple stages of igneous rocks occur in the recently discovered Nianzigou Mo deposit in Chifeng, Inner Mongolia, which can provide insights into the late Mesozoic geodynamic evolution of the southern Da Hinggan Range. The mineralization age is similar to the age of local granites, but there are few detailed studies of the tectonic setting during Cu-Mo mineralization in this area. The Nianzigou Mo deposit is located close to the northern margin of the North China Craton and in the eastern Central Asian Orogenic Belt and is a typical quartz-vein-type Mo deposit in the Xilamulun Mo ore belt. The granite in this deposit has high SiO₂, Al₂O₃, K₂O, and Na₂O contents, and low MgO, CaO, and Fe₂O₃^t contents. The granite is characterized by enrichments in large-ion lithophile elements and depletions in high-field-strength elements and, in particular, Sr, Ti, and P. The granite has high contents of rare-earth elements, is enriched in light rare-earth elements, and has marked negative Eu anomalies. The granite is an alkaline and calc-alkaline and metaluminous A-type granite. The zircon U-Pb ages of the monzogranite and granite porphyry are 157.2 ± 0.3 and 154.4 ± 0.4 Ma. The model age obtained by Re-Os isotopic dating is 154.3 ± 1.7 Ma, indicating that molybdenite mineralization also occurred during the Late Jurassic period. Given that the molybdenite Re contents are 7.8–24.9 ppm (average = 16.8 ppm), the ore-forming materials of the Nianzigou Mo deposit had a mixed crust–mantle source, but were mainly derived from the lower crust. Based on the geology and geochemistry, we propose that the Nianzigou Mo deposit formed in a postorogenic extensional tectonic setting associated with the southward subduction of the Mongol–Okhotsk oceanic plate.

Keywords: geochronology; zircon U-Pb dating; postcollisional; A-type granite; Late Jurassic; Nianzigou Mo deposit



Citation: Li, Y.; Yang, Y.; Hua, L.; Leng, Y.; Xin, J. Geochronology and Tectonic Implications of the Nianzigou Granites and Associated Mo Deposit, Inner Mongolia. *Minerals* **2022**, *12*, 791. <https://doi.org/10.3390/min12070791>

Academic Editors: Victoria B. Ershova, Artem V. Moiseev and Andrey Khudoley

Received: 14 April 2022

Accepted: 15 June 2022

Published: 21 June 2022

Publisher's Note: MDPI stays neutral with regard to jurisdictional claims in published maps and institutional affiliations.



Copyright: © 2022 by the authors. Licensee MDPI, Basel, Switzerland. This article is an open access article distributed under the terms and conditions of the Creative Commons Attribution (CC BY) license (<https://creativecommons.org/licenses/by/4.0/>).

1. Introduction

The eastern margins of the cratons in China contain an extraordinary mineral endowment, related to the tectonic setting and processes in this region [1–6]. Vast Mo ore resources occur along the margin of the North China Craton (NCC). The Yan–Liao Mo ore belt in the NCC and the East Qinling Mo ore belt along the southern margin of the NCC are two renowned Mo ore belts, and account for >60% of the proven Mo reserves in China [7–12]. Therefore, studies of the ore-controlling factors and specific Mo mineralization mechanisms in these deposits are important for future exploration and exploitation.

Northeast China is located in the eastern Central Asian Orogenic Belt (CAOB, Figure 1a), with the NCC to the south and Siberian Craton to the north. A number of porphyry Cu-Mo deposits of late Paleozoic to Mesozoic ages have been discovered in recent years, such as the Chehugou, Yuanbaoshan, Jiguanshan, and Nianzigou deposits. Their mineralization ages vary between 260 and 130 Ma, and are similar to those of nearby granites [13–23]. To date, there have been no detailed studies on the origins, structures, mineralization mechanisms, and tectonic settings of Cu-Mo deposits in this area.

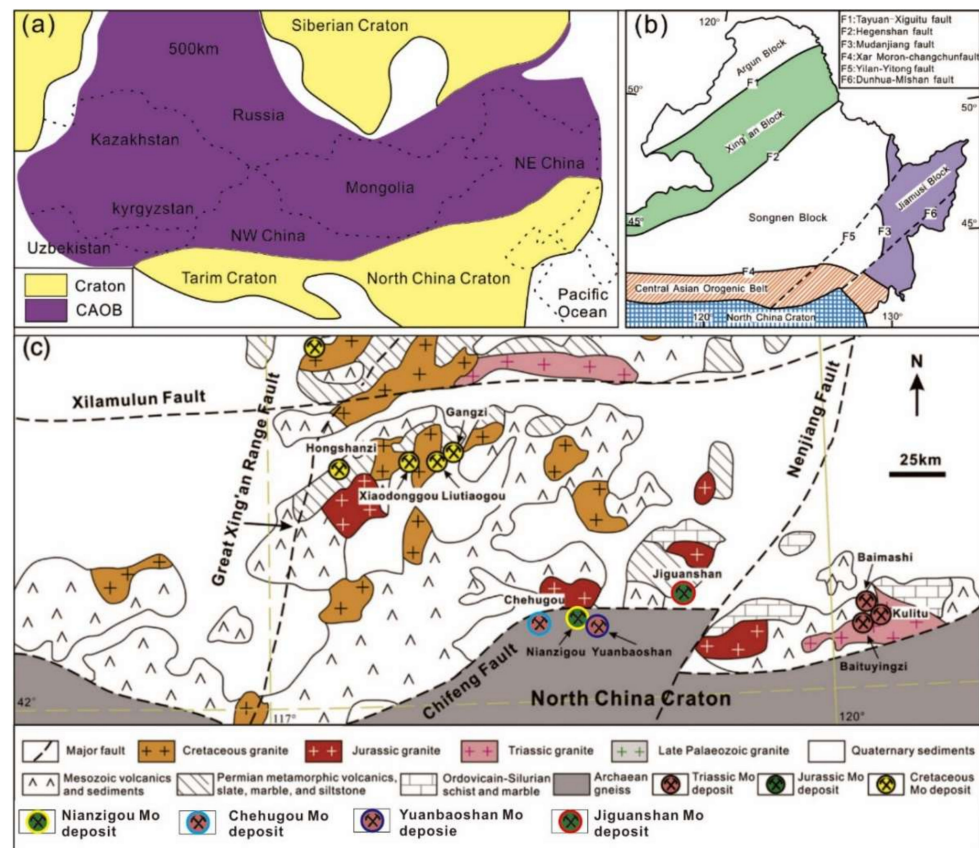


Figure 1. (a) Schematic map of the Central Asian Orogenic Belt. (b) Tectonics subdivisions of northeastern China and location of the North China Craton (NCC) and the Central Asian Orogenic Belt. (c) Regional geological map of the geological setting and the locations of major Mesozoic Mo deposits (modified after Shu et al., 2015) [10].

Mesozoic granites associated with Mo deposits are widely distributed along the northern margin of the NCC in northeast China and in the Da Hinggan Range (Figure 1c). One important question is why most Mo deposits formed during the Cretaceous period in the Da Hinggan Range, but are older (Triassic–Jurassic) near the margin of the NCC. Due to the limited occurrences of igneous rocks, the tectonic setting of the northern margin of the NCC at this time remains poorly understood.

In this study, biotite monzogranite and granite porphyry in the Nianzigou Mo deposit were collected for zircon U–Pb dating as well as the gathering of molybdenite Re–Os isotope age data to better constrain the relationship between magmatism and Mo mineralization. This paper focuses on the ore-bearing granite and ore body in the ore belt, and combined with the complex tectonic evolution from the Late Paleozoic to early Mesozoic periods in the northern margin of NCC, we understand the characteristics, genesis, and geodynamic background of this series of copper molybdenum deposits, as well as the metallogenic specificity of granite and copper molybdenum deposits.

2. Geological Setting

The Nianzigou Mo deposit is located 25 km to the northwest of Chifeng City, Inner Mongolia. It is located in the CAOB between the Siberian Craton and NCC (Figure 1c). Northeastern China is generally considered to be in the eastern CAOB, which consists of several microcontinental fragments (Figure 1b) [15,17]. The Da Hinggan Range has experienced successive tectonic events (i.e., orogenies) that were mainly controlled by the evolution of the Paleo-Asian Ocean during the Paleozoic, Mongol–Okhotsk Ocean during the late Paleozoic to late Mesozoic periods, and Paleo-Pacific Ocean during the late Mesozoic period [24–26]. The fault structures in the study area mainly trend east–west

and (north)-northeast-(south)-southwest. In addition, there are some small secondary faults. The Xilamulun Fault is a significant fault in the northern part of this area that trends east–west. This fault is considered to represent the suture between the North China and Siberian cratons [27–30]. The fault extends southward to the NCC, where it is called the Wendurmiao–Wengniute Caledonian accretionary belt, and northward to the Erlian–Hegenshan structural belt, where it is called the Variscan accretionary belt in the southern Da Hinggan Range. The east–west trending Chifeng–Kaiyuan Fault is a major fault in the southern part of this area and is a compressive torsional fault. This fault is considered to be the boundary between the NCC and the Tianshan–Xingmeng fold belt. North of the fault is the Xingmeng orogenic belt.

In this region, magmatism has occurred during the Hercynian, Indosinian, and Yanshanian events (e.g., Devonian–Carboniferous magmatism for the Hercynian event, Triassic to Early Jurassic magmatism for the Indosinian event, and Jurassic to Early Cretaceous magmatism for the Yanshanian event). The Hercynian igneous rocks are mainly syenogranite, quartz diorite, and granodiorite; the Indosinian igneous rocks comprise mainly granite porphyry and monzogranite; and the Yanshanian igneous rocks are mainly biotite granite, monzogranite, granodiorite, and granite porphyry. These three stages of magmatism were mainly intruded as batholiths, stocks, and dikes. The Yanshanian igneous rocks are generally better exposed, and exhibit some zoning in terms of their spatial distribution. In general, the Yanshanian igneous rocks are linearly distributed along both sides of the Xilamulun and Chifeng–Kaiyuan faults (Figure 1b). In recent years, mineral exploration has discovered that some granites are closely related to Cu–Mo mineralization in this region [28–31]. A-type granite plutons in this region were associated with lithospheric thinning and were derived from the lower crust [26,32]. The magmatism also had a close temporal and spatial relationship with Mo mineralization in the southern Da Hinggan Range.

3. Ore Deposit Geology

The Nianzigou Mo deposit is located in the southern Da Hinggan Range mineralization belt (Figure 1c). The main rock types exposed in this region are Mesozoic intrusive rocks and Quaternary sediment. The Paleozoic Baoyintu Group epimetamorphic rocks are poorly exposed (Figure 1c). The regional faults that trend nearly east–west control the distribution of igneous rocks.

Magmatism in the Da Hinggan Range mineralization belt is of Indosinian and Yanshanian ages and is closely related to Mo mineralization. The nearby Chehugou Cu–Mo and Kulitou Mo deposits formed in the Indosinian age [32], and the Jiguanshan Mo deposit formed in the Yanshanian age [33]. The exposed outcrop area of the Yanshanian medium- to coarse-grained biotite monzogranite in the Nianzigou Mo deposit is around 120 km². The distribution of outcrops is generally controlled by regional northeast–southeast-trending faults. The Archean Jianping Group comprises amphibolitic gneiss, biotite amphibolite, and amphibolite, which are exposed around the biotite monzogranite. The mafic volcanic rocks of the Cretaceous Yixian Formation (K_{1y}) comprise volcanic rocks, volcanic breccias, agglomerates, and tuffs. Cenozoic basalts also crop out in this region.

The ore-bearing rock unit is oval-shaped in plan view, with dimensions of around 20 km from east to west and around 15 km from north to south. Granite porphyry and lamprophyre dikes occur in the biotite monzogranite (Figure 2). The monzogranite is light gray–brown in color, medium- to fine-grained with an irregular grain size, and massive in structure (Figure 3a,b). The monzogranite consists of quartz, plagioclase, K-feldspar, and biotite, along with accessory titanite, ilmenite, and magnetite.

The monzogranite has been intruded by granite porphyry and lamprophyres along the northeastern side of the mining area. These secondary intrusives are 100–1200 m in length, 3–8 m in width, and trend north–northwest–south–southeast and dip 60–80° to the west. The granite porphyries are dark gray in color, porphyritic, and massive. They consist mainly of quartz, plagioclase, and K-feldspar, which have undergone intense alterations including sericitization and carbonatization of plagioclase (Figure 3c,d). The lamprophyres

are dark grayish green in color, porphyritic, and massive. They consist mainly of biotite, amphibole, plagioclase, and pyroxene, which have also been strongly altered, including chloritization of biotite and amphibole, and kaolinization and carbonatization of plagioclase (Figure 3d,e).

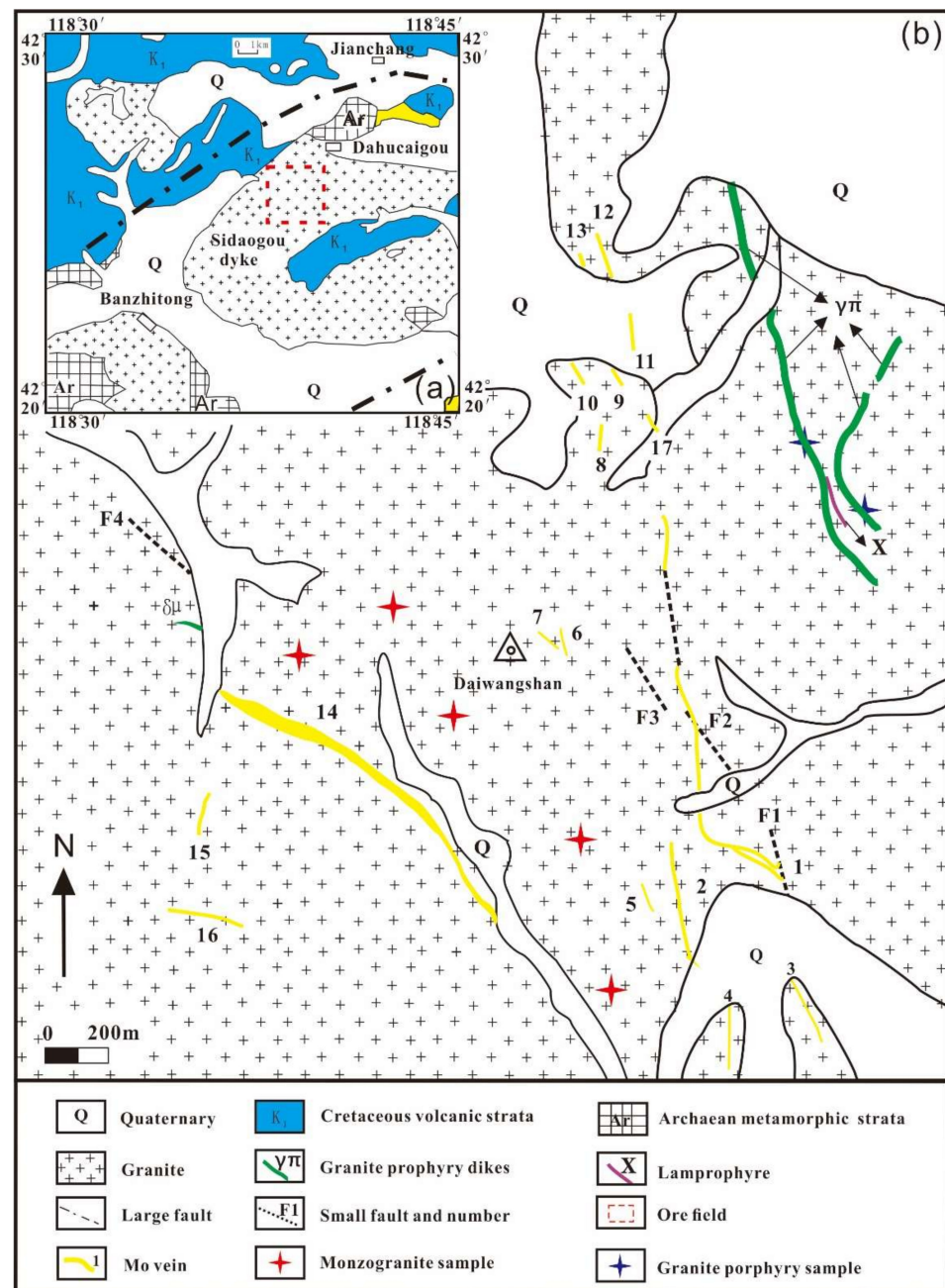


Figure 2. Geological sketch map of the host granite and the Nianzigou Mo deposit. (a) Deposit location, (b) ore vein distribution (modified after Chen et al., 2008) [16].

Molybdenum orebodies occur along mineralized alteration zones and are linearly distributed along fracture and fault zones within and at the margins of the monzogranite. The mineralized-related alteration includes mainly silicification, sericitization, and potassic types. Silicification produced white, solid quartz veins and veinlets, and disseminated pyroxene. Sericitization occurred in the rocks surrounding the orebodies, where sericite occurs with K-feldspar and, in some cases, fine-grained molybdenite. Potassic alteration formed automorphic crystals of red K-feldspar in the rocks surrounding the orebodies and

is associated with sericite and fine-grained molybdenite. The mineralization occurs mainly as Mo-rich veins (at depth) and is accompanied by Cu-Mo mineralization in the upper part of the deposit.

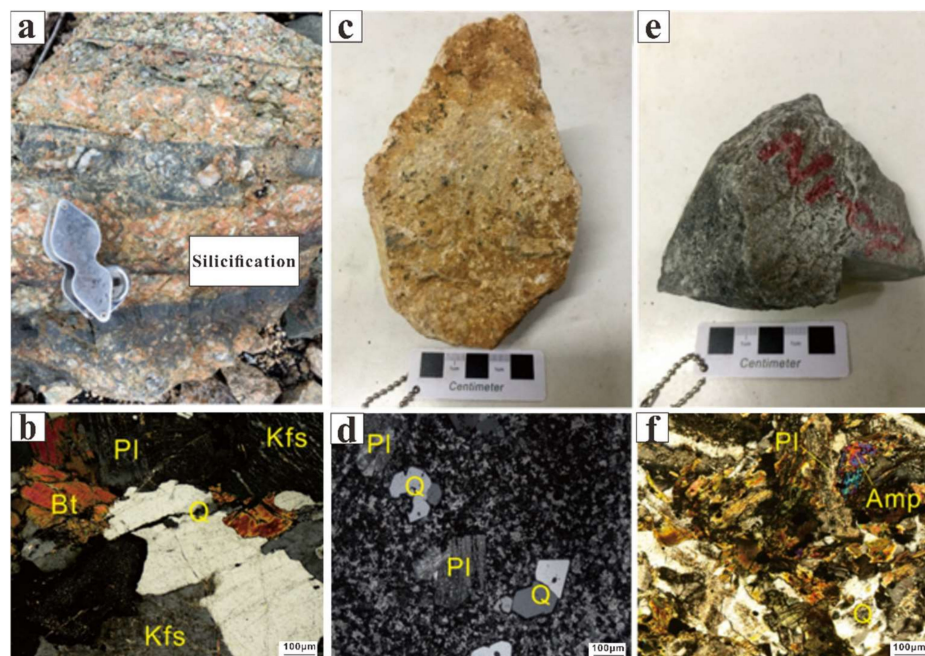


Figure 3. Photos and photomicrographs of representative granite from the Nianzigou district. (a) Biotite monzogranite, (b) Biotite monzogranite under cross-polarized light; (c) Granite porphyry dyke, (d) Granite porphyry dyke under cross-polarized light; (e) Diorite porphyrite dyke, (f) Diorite porphyrite dyke under cross-polarized light. Kfs = K-feldspar, Pl = plagioclase, Bt = biotite, Q = quartz, Amp = amphibole.

4. Samples and Analytical Methods

Seven fresh granitic rock samples, including monzogranite and granite porphyry, were collected from the mining area, $118^{\circ}39'00''$ E, $42^{\circ}26'00''$ N. The monzogranite and granite porphyry samples were used for zircon U-Pb dating. Seven samples were selected for whole-rock analyses. Six molybdenite samples were selected for Re-Os isotopic analyses. The petrographic characteristics of the samples are presented in Figure 3.

4.1. Zircon U-Pb Dating

Zircon crystals were separated at the Yantuo Geologic Service Co. Ltd., Langfang, China. Zircons were separated by magnetic and heavy liquid methods after the samples were crushed. Euhedral–subhedral zircon crystals with no cracks and inclusions were handpicked under a binocular microscope. Internal structures in the zircon crystals were imaged by cathodoluminescence (CL) techniques.

Zircon U-Pb dating and trace-element analysis were carried out by laser ablation inductively coupled plasma mass spectrometry (LA-ICP-MS) at Shangpu Geologic Analysis Service Co. Ltd., Wuhan, China. Analyses were conducted using an Aurora M90 ICP-MS coupled to a New Wave UP 213 LA system. The samples were analyzed with a laser beam diameter of $30\ \mu\text{m}$, ablation rate of 10 Hz, and laser energy density of $2.5\ \text{J}/\text{cm}^2$. The carrier and make-up gases were He and Ar, respectively [34,35]. Age calibrations were undertaken using the standard zircon reference material 91,500. Zircon trace-element contents were quantified by using SRM610 as the external standard, with Si as an internal standard. The methods reported in Andersen [36] were used for common Pb correction. The isotope ratios and elemental contents were calculated using the ICP-MS-DATCAL program. Concordia plots and weighted-mean ages were calculated using Isoplot (Version 3.0, [37]). Zircon

U-Pb isotopic and trace-element data are presented in Supplementary Tables S1 and S2, respectively.

4.2. Molybdenite Re-Os Dating

Six molybdenite samples were collected for Re-Os dating. Molybdenite was magnetically separated and handpicked under a binocular microscope to ensure a purity of >99%. The Re-Os isotope analyses were carried out at the Re-Os Isotope Laboratory, National Research Center of Geoanalysis, Chinese Academy of Geological Sciences (CAGS), Beijing, China. Detailed procedures have been described in Du et al. [38]. Data quality was assessed by analyses of the JDC standard certified reference material GBW04436. The molybdenite Re-Os model ages were calculated as follows: $t = \lambda^{-1} [\ln (1 + {}^{187}\text{Os}/{}^{187}\text{Re})]$, where λ is the ${}^{187}\text{Re}$ decay constant ($1.666 \times 10^{-11} \text{ yr}^{-1}$). Isoplot/Ex version 3.0 [37] was used to calculate the Re-Os isochron age. The Re-Os isotopic data are listed in Supplementary Materials Table S3.

4.3. Whole-Rock Major- and Trace-Element Geochemistry

The least-altered rock samples were crushed, cleaned with deionized water, and powdered to 200 mesh in an agate mill. Sample processing and major- and trace-element analyses were undertaken at the State Key Laboratory of Geological Processes and Mineral Resources, China University of Geosciences, Beijing, China. Major-element compositions were determined by X-ray fluorescence (XRF) spectrometry. Trace-element compositions were determined using an Agilent 7500a ICP-MS. The analytical precision was $< \pm 5\%$ for major elements and $< \pm 10\%$ for trace elements, which was constrained by analyses of the international standards BHVO-2 and BCR-2, and national standards GBW07103 and GBW07104. The major-element data are presented in Supplementary Materials Table S4.

5. Results

5.1. Zircon U-Pb Ages

Nearly all zircon grains from samples N3-1 (monzogranite) and N2-4 (granite porphyry) are transparent and euhedral-subhedral, showing magmatic oscillatory growth zonation in cathodoluminescence (CL) images (Figure 4).



Figure 4. Cathodoluminescence (CL) images of the Nianzigou granite.

Twenty analyses were undertaken on zircons from both the monzogranite and granite porphyry. The obtained data and concordia ages are presented in Supplementary Materials Table S1. The zircon Th and U contents vary considerably. The granite porphyry sample has zircon Th contents of 114–626 ppm, U contents of 104–691 ppm, and Th/U = 0.69–2.13. The monzogranite sample has zircon Th contents of 293–1494 ppm, U contents of 450–1380 ppm, and Th/U = 0.45–1.29. The Th and U data are typical of magmatic zircon [39–41].

The granite porphyry sample yielded 20 reliable ${}^{206}\text{Pb}/{}^{238}\text{U}$ ages of 150.0 ± 2.4 to 160.0 ± 2.4 Ma, with a weighted-mean age of 154.4 ± 0.4 Ma (MSWD = 0.29). In a ${}^{206}\text{Pb}/{}^{238}\text{U}$ - ${}^{207}\text{Pb}/{}^{235}\text{U}$ concordia diagram (Figure 5a), the U-Pb isotopic data fall on or plot close to the concordia, indicating that the zircons were not affected by later thermal events.

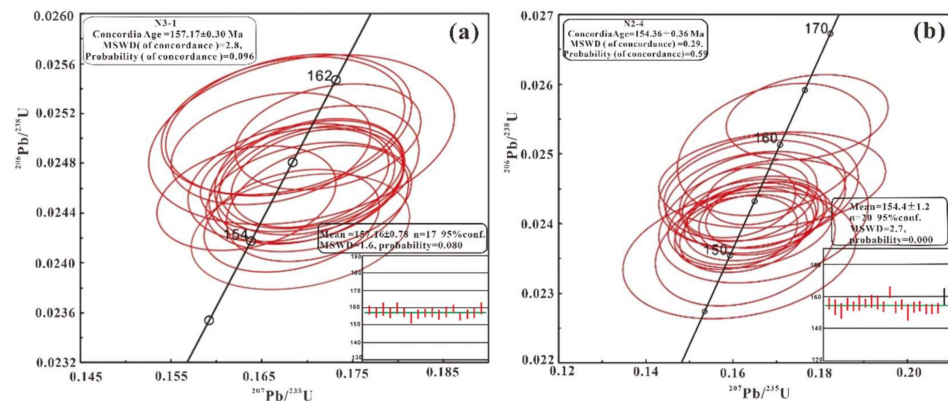


Figure 5. U-Pb concordia diagrams showing the LA-ICP-MS zircon dating results of the Nianzigou monzogranite (a), and granite porphyry (b).

The monzogranite sample yielded 16 reliable $^{206}\text{Pb}/^{238}\text{U}$ ages of 155.0 ± 1.1 to 160.0 ± 1.5 Ma, with a weighted-mean age of 157.2 ± 0.3 Ma (MSWD = 2.8), which indicates that its emplacement occurred in the Late Jurassic period. These U-Pb isotopic data are also concordant (Figure 5b). The granite porphyry age is younger than the monzogranite age, which is consistent with the granite porphyry having intruded the monzogranite, indicating that the results are robust and that the ages of the igneous rocks in the Nianzigou Mo deposit are ca. 155 Ma.

5.2. Molybdenite Re-Os Dating

To examine the relationship between magmatism and Mo mineralization in the Nianzigou deposit, it is necessary to obtain geochronological data for the mineralization.

The Re and common Os concentrations are 7839–24,930 and 12.62–40.37 ng/g, respectively (Supplementary Materials Table S3). Six molybdenite samples show consistent Re-Os model ages, ranging from 152.7 ± 2.1 to 155.5 ± 2.5 Ma, and yield a well-constrained $^{187}\text{Re}/^{187}\text{Os}$ isochron age of 154.3 ± 1.7 Ma (MSWD = 1.4). Using the ISOPLOT/Ex program [36], the data yielded an isochron age of 154.3 ± 1.7 Ma and an initial ^{187}Os of -0.06 ± 0.21 ng/g, and a weighted-mean age of 153.93 ± 0.89 Ma (MSWD = 0.65) (Figure 6).

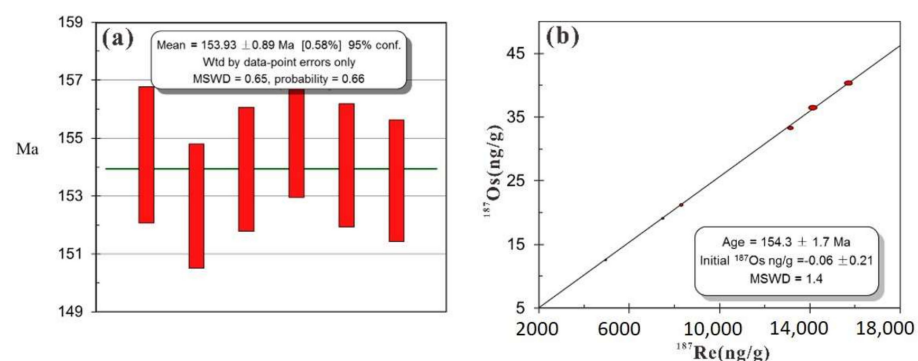


Figure 6. Weighted mean ages (a) and isochron Re-Os ages (b) of molybdenites from the Nianzigou Mo deposit.

5.3. Whole-Rock Geochemistry

The SiO_2 contents of four biotite monzogranites are 69.24–72.67 wt% (average = 71.23 wt%), and these samples are silica-oversaturated. Al_2O_3 contents vary from 12.89 to 13.58 wt% (average = 13.33 wt%). The Na_2O , K_2O , and total alkali contents are 3.73–4.07, 3.99–4.70, and 7.90–8.43 wt%, respectively. The MgO , CaO , and Fe_2O_3^t contents are 0.61–1.59, 1.14–2.15, and 2.28–4.64 wt%, respectively. The SiO_2 and Al_2O_3 contents of the granite porphyry are 73.10 and 13.08 wt%, respectively. The Na_2O and K_2O contents are 3.68 and 4.66 wt%,

respectively. The MgO, CaO, and Fe₂O₃^t contents are 0.65, 1.40, and 2.54 wt%, respectively, and are slightly lower than those of the biotite monzogranites. The SiO₂ contents of samples N3-1 (granite porphyry) and N3-4-1 (biotite monzogranite) are very high (>80 wt%), and obviously different from the other samples. Given the SiO₂ content, N3-1 maybe a different intrusion from the other granite porphyry.

Trace-element data are presented in Supplementary Materials Table S2, and chondrite-normalized REE and primitive-mantle-normalized trace-element patterns are shown in Figure 7a. The total REE (Σ REE) contents of the analyzed monzogranites are high, with Σ REE = 183.59–258.15 ppm (average = 213.89 ppm). Total light REE (Σ LREE) contents are 171.65–239.15 ppm (average = 198.47 ppm), and total heavy REE (Σ HREE) contents are 12.81–19.00 ppm (average = 15.42 ppm). (La/Yb)_N ratios vary from 13.74 to 16.08 (average = 14.77) and the monzogranites have moderate negative Eu anomalies (Eu/Eu* = 0.63–0.70; average = 0.67). The granite porphyry has Σ REE = 103.34 ppm, Σ LREE = 97.08 ppm, Σ HREE = 6.26 ppm, (La/Yb)_N = 16.66, and Eu/Eu* = 0.63. The biotite monzogranites and granite porphyry have similar REE patterns, which are LREE-enriched. All five samples exhibit obvious negative Eu anomalies, indicating significant fractional crystallization of plagioclase or K-feldspar during magma ascent. The biotite monzogranites and granite porphyry are enriched in large-ion lithophile elements (LILEs), such as Rb, Ba, Sr, and K, and depleted in high-field-strength elements (HFSEs), such as Nb, Ta, and Ti (Figure 7b).

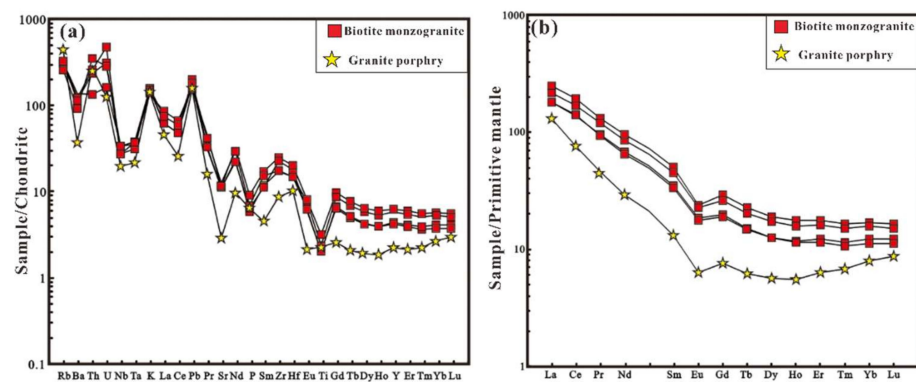


Figure 7. Primitive mantle-normalized trace-element spider diagram (a) and chondrite-normalized rare-earth-element pattern (b) for the Nianzigou granite (Sun and McDonough, 1989) [40].

6. Discussion

6.1. Classification of the Nianzigou Granite

A-type granites are typically alkaline and anhydrous, and formed in extensional tectonic settings [21]. A-type granites generally have higher HFSE contents ($Zr + Nb + Ce + Y > 350$ ppm), Ga/Al ratios ($10,000 \times Ga/Al > 2.6$), total alkali contents ($Na_2O + K_2O > 8$ wt%), and FeO^t/MgO ratios (>4.0) than other granite types [22]. The Nianzigou monzogranite is alkaline–calc-alkaline (Figure 8a,c), and has high $10,000 \times Ga/Al$ ratios (3.1–4.8), $K_2O + Na_2O$ contents (8.9–9.4 wt%), and $Zr + Nb + Ce + Y$ contents (350–600 ppm) (Figure 8c,d). The monzogranites also have higher FeO^t/MgO ratios (4–12; Figure 8b) than the I-type (average = 2.2), M-type (average = 2.3), and S-type (average = 2.3) granites [22]. Most samples of the Nianzigou monzogranite plot in the A-type field in discrimination diagrams.

On a SiO₂ versus ($Na_2O + K_2O$) classification diagram both the biotite monzogranite and granite porphyry plot in the granite field (Figure 9a), which is consistent with the hand-sample and thin-section observations. On an A/CNK versus A/NK diagram, most of the samples plot in the metaluminous field (Figure 9b). In other magmatic discrimination diagrams (Figure 9c,d), all the samples plot in the high-K calc-alkaline field.

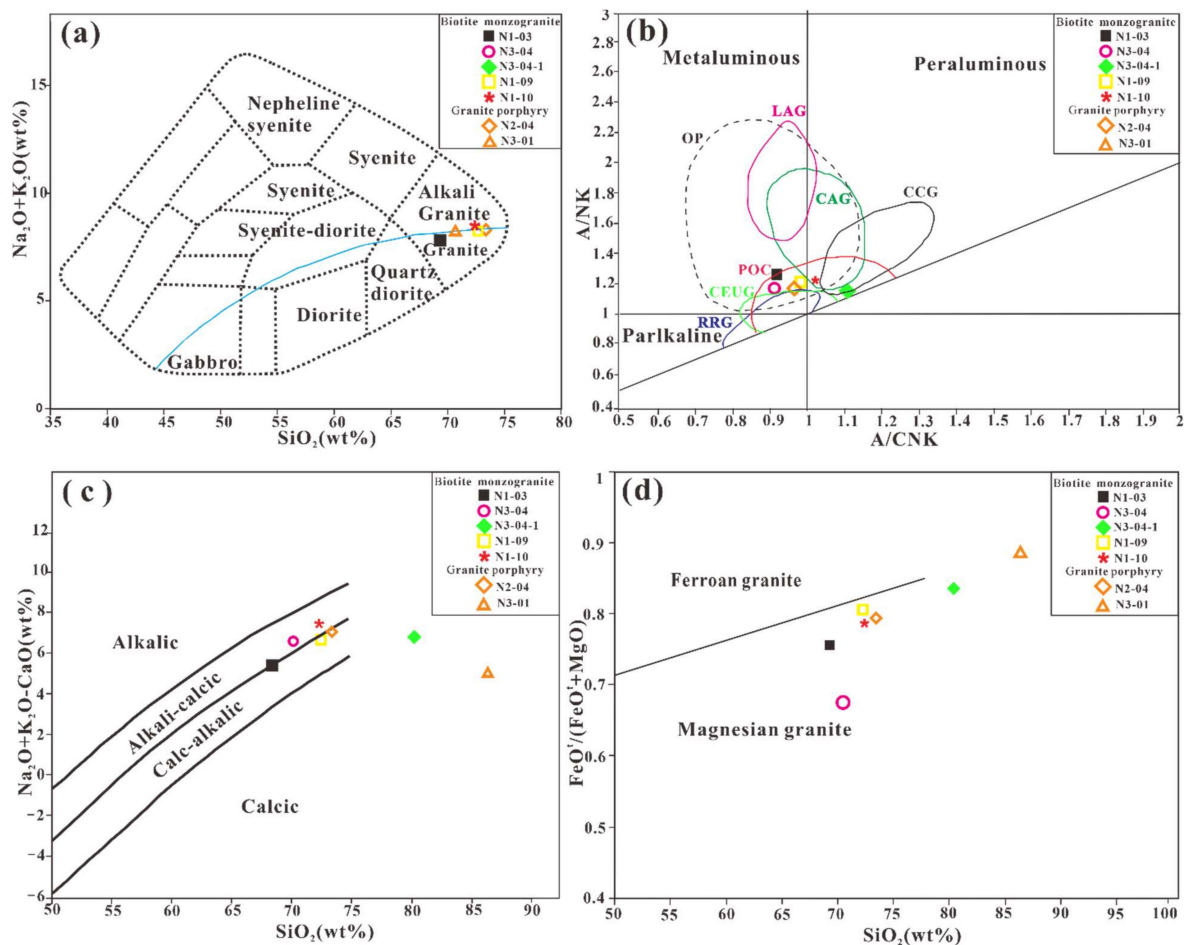


Figure 8. Major element diagrams for the Nianzigou granite. (a) Total alkalis versus silica diagram (after Middlemost [41]). (b) A/NK vs. A/CNK diagram (after Pearce [42]). (c) $\text{Na}_2\text{O} + \text{K}_2\text{O} + \text{CaO}$ vs. SiO_2 diagram (after Peccerrior [43]). (d) $\text{FeO}^t/(\text{FeO}^t + \text{MgO})$ vs. silica diagram (after Frost and Frost [44]).

6.2. Source and Petrogenesis of the Nianzigou Monzogranite

There are three petrogenetic models for the origins of A-type granites: (1) differentiation of mantle-derived alkaline basalts [45,46]; (2) partial melting of various crustal sources; and (3) mixing between mantle-derived magma and crustal melts [22,47–49].

The Nianzigou A-type monzogranite has high SiO_2 contents (69.24%–73.10%) and low Mg# values (0.16–0.34), which indicate that it was not derived from the mantle (mantle-derived alkali silicic magmas have $\text{Mg}\# = 0.47\text{--}0.76$) [46]. In addition, no coeval mafic-intermediate rocks have been found in this area [50], implying that the Nianzigou monzogranite was not formed by fractional crystallization of a mantle-derived magma.

Melting of metasedimentary rocks is an unlikely origin for the Nianzigou monzogranite, because it has lower initial $^{87}\text{Sr}/^{86}\text{Sr}$ ratios (0.7069–0.7091) than metasedimentary rock-derived A-type granites (>0.715) [51,52]. Moreover, A-type granites derived by melting of metasedimentary rocks are peraluminous, whereas the Nianzigou A-type monzogranite is metaluminous to weakly peraluminous ($\text{A}/\text{CNK} = 0.98\text{--}1.07$, Figure 9b). Oxidized and reduced A-type granites can be discriminated in a $\text{FeO}^t/(\text{FeO}^t + \text{MgO})$ versus Al_2O_3 diagram (Figure 10a) [53]. The Nianzigou A-type monzogranite has compositional characteristics that differ from those of reduced A-type granites (Figure 10a), which indicates that they were not derived from differentiated tholeiitic sources. The geochemical characteristics of the biotite monzogranite and granite porphyry are similar, and these rocks only have different occurrences.

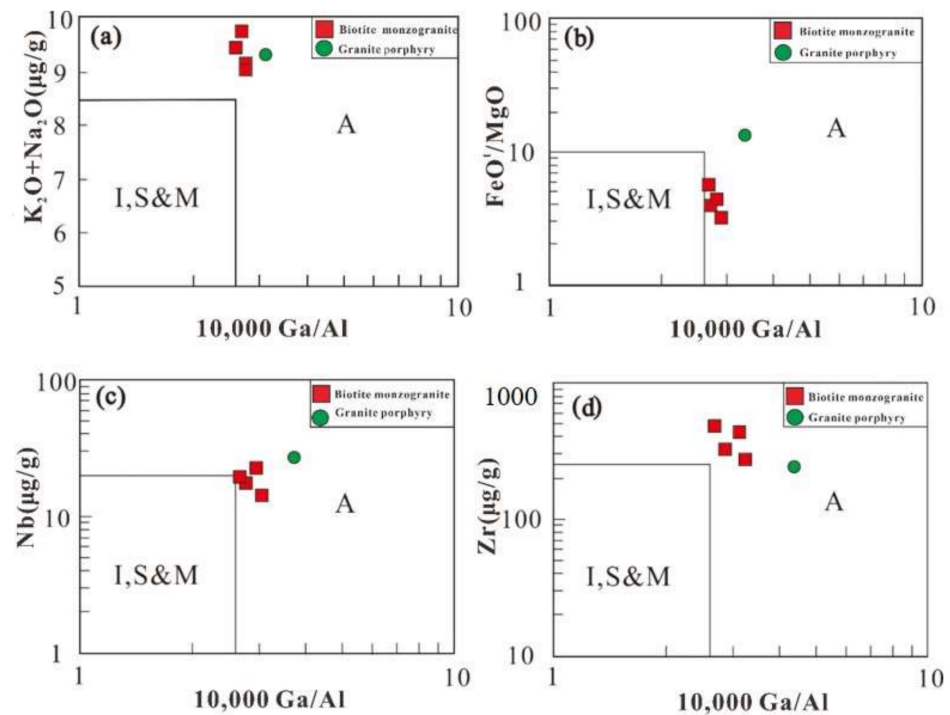


Figure 9. Plots of $K_2O + Na_2O$ vs. $10,000 \times Ga/Al$ (a), FeO^t/MgO vs. $10,000 \times Ga/Al$ (b), Nb vs. $10,000 \times Ga/Al$ (c), Zr vs. $10,000 \times Ga/Al$ (d) classification diagrams for the Nianzigou granite (after Whalen et al. [22]).

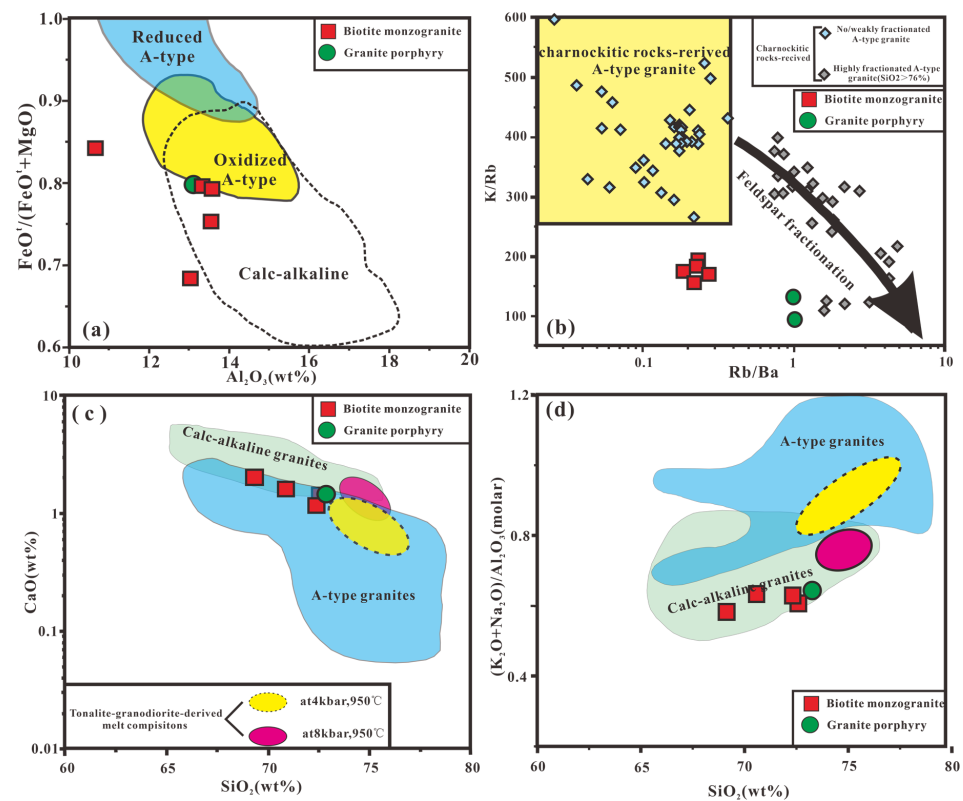


Figure 10. (a) Plots of Al_2O_3 vs. $FeO^t/(FeO^t + MgO)$ (after Dall’Agnol and de Oliveira, 2007 [53]). (b) Rb/Ba vs. K/Rb . (c) SiO_2 vs. CaO . Data sources for charnockitic rocks derived from A-type granite were after Landenberger and Collins, 1996; Zhao et al., 2008; Ji et al., 2019b [47,48,54]. (d) SiO_2 vs. molar $(Na_2O + K_2O)/Al_2O_3$ (tonalite–granodiorite-derived melt compositions and dates of A-type granites and calc-alkaline granitoids were after Patiño Douce [49]).

6.3. Tectonic Setting

Although the origins of A-type granites are controversial, it is generally accepted that they form in postorogenic and/or anorogenic settings characterized by lithospheric extension [22]. It is difficult to distinguish postorogenic and anorogenic tectonic settings using A-type granites [23].

Patiño-Douce [49] noted that calc-alkaline rocks can form silica-rich A-type granites by dehydration melting of biotite in the upper crust (≤ 4 kbar). A-type granites form at low pressures and shallow depths (<15 km). The melting of tonalite at <0.8 GPa can generate A-type granites [22], with low Al_2O_3 and high Y, Nb, and HREE contents, and marked negative Eu and Sr anomalies.

Studies of Mesozoic granites that are widely distributed along the northern margin of the NCC, and in northeast China and the Da Hinggan Range have concluded that most are A-type granites. Liu et al. [55] suggested that the Mesozoic granites along the northern margin of the NCC are the result of strong crust–mantle interactions during and after a continental collision event that transitioned to an intraplate anorogenic stage. Lin et al. [56] proposed that during closure of the Mesozoic Paleo-Asian Ocean, magma generated by the partial melting of alkaline mafic rocks promoted the partial melting of pre-existing lower crust or that differentiation of mantle-derived basaltic magma occurred during underplating. Other studies have suggested that the A- and some I-type granites were formed by decompression melting of the asthenospheric mantle due to lithospheric thinning after a collisional orogeny, and that these magmas experienced relatively little crustal contamination. Alternatively, during lithospheric extension, underplating of mantle-derived mafic magma caused melting of the juvenile lower crust or was contaminated by ancient lower crust [31].

On Y/Nb versus Rb/Nb (Figure 11a) and Nb–Y–Ce ternary (Figure 11b) diagrams, the data plot in the postorogenic field, similar to Late Jurassic–Early Cretaceous A-type granites from the northern margin of the NCC. This result, and the similar major- and trace-element features of the studied samples and Mesozoic A-type granites from the northern margin of the NCC and in northeast China, suggest they have a similar origin. Previous studies have shown that, after the early Mesozoic period, the northern margin of the NCC entered a postorogenic stage. We speculate that during postorogenic lithospheric extension, the crust–mantle transition zone underwent decompression melting, generated primitive magma, and this magma then experienced crustal contamination, which formed the A-type Nianzigou granites. The obvious difference in the Nd isotopic compositions between the studied granites and those located farther east may be because the study area is closer to the NCC and was contaminated by older continental crustal materials. Chen et al. [27] reported that the $(^{87}\text{Sr}/^{86}\text{Sr})_i$ ratios of the ore-bearing Nianzigou granite are low (0.70516–0.70519), its $\varepsilon_{\text{Nd}}(t)$ values are negative (−3.8 to −7.4), and its Pb isotopic compositions are characteristic of the lower crust [16].

In general, the variation of Sr and Nd isotopes can reflect the assimilation of the crustal component during magma ascent. The coexistence of assimilation and fractional crystallization (AFC) can lead to an increase in the SiO_2 content and the $(^{87}\text{Sr}/^{86}\text{Sr})_i$ value and a decrease in the $\varepsilon_{\text{Nd}}(t)$ value during the magma evolution [48]. Therefore, the linear relationship between the Sr and Nd isotopes and the SiO_2 content can reflect the AFC process. Adjacent to the Chehugou deposit area, the positive correlation between the SiO_2 content and the $(^{87}\text{Sr}/^{86}\text{Sr})_i$ value and the negative correlation between the SiO_2 content and the $\varepsilon_{\text{Nd}}(t)$ value indicate that the assimilation of the crust occurred during magma evolution.

Based on the trace-element tectonic discrimination diagram for granites of Pearce et al. [42] the Nianzigou monzogranite had a within-plate tectonic setting (Figure 11). The thick subcontinental lithospheric mantle of the cold buoyant cratons helped to preserve some of the world's oldest porphyry-skarn and epithermal mineral deposits. The available geochemical and isotopic data suggest that the ore-forming porphyries were produced

by partial melting of juvenile lower crust that resulted from basaltic underplating in an intracontinental extensional setting.

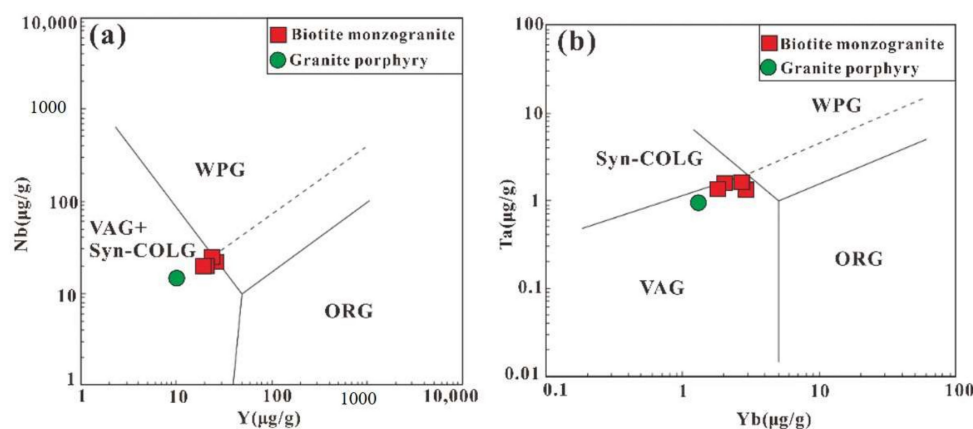


Figure 11. Discrimination diagram of the granite tectonic environment. Nb vs. Y diagram (a) and Ta vs. Yb diagram (b). Diagrams after Pearce et al. [42]). Fields for syncollision (COLG), volcanic-arc (VAG), within-plate (WPG), and ocean-ridge (ORG) granites are indicated.

A-type granites can be further subdivided into the A₁ and A₂ groups: the former is typically related to an anorogenic setting, and the latter is associated with a postorogenic tectonic setting. All the granitic rocks belong to the A₂ type, indicating a postorogenic tectonic setting related to the Mongol–Okhotsk orogeny. Moreover, a large number of rift basins (e.g., the Erlian basin in the western area, the Songliao basin in the eastern area, Figure 1b) and bimodal volcanic rocks and A-type granites from the Late Jurassic to Early Cretaceous periods are widespread on both sides of the Da Hinggan Range [31]. These geological observations, together with the geochemical signatures, provide robust evidence of the postorogenic extensional tectonic setting. Combined with the spatial distribution of the different types of deposits and volcanic intrusive rocks, the rift basins, and the tectonic deformation styles in the Late Jurassic period, which constitute a typical basin-range structure formed in the postorogenic tectonic setting, we suggest that the Late Jurassic Mo polymetallic mineralization and related granites formed in an extensional environment linked to the postorogenic collapse of the Mongol–Okhotsk orogeny between the Mongolia–North China block and the Siberia Block.

6.4. Timing of Magmatism and Mineralization

Molybdenum deposits and granites related to mineralization in the Xilamulun mineralization belt (i.e., the Chifeng area), along the northern margin of the NCC, have ages that are mainly concentrated in three periods: (1) 260–220 Ma [33], such as the Chehugou Cu-Mo and Yajishan Mo deposits; (2) 180–150 Ma, such as the Nianzigou Mo deposit; and (3) 140–120 Ma, such as the Xiaodonggou Mo deposit. Given the tectonic history of the northern margin of the NCC, it is speculated that these three stages of mineralization were related to a collisional orogeny, postorogenic extension, and intracontinental extension, respectively. The mineralization periods of 180–150 and 140–120 Ma are similar to the mineralization ages of the Yan–Liao Mo-(Cu) deposits from the northern margin of the NCC. However, no Mo mineralization of the late Permian to early Triassic age has been found in the Yan–Liao area, which may be because this area is closer to the interior of the NCC. The late Permian to early Triassic mineralization may be related to the closure of the Paleo-Asian Ocean and subsequent collisional orogeny. The age of the Nianzigou granite in the study area is 157 Ma, and studies of this deposit may provide further insights into the important Late Triassic to Late Jurassic (180–150 Ma) Mo mineralization along the northern margin of the NCC.

7. Conclusions

- (1) The granites in the Nianzigou Mo deposit yielded zircon U-Pb ages of 157.2 ± 0.3 and 154.4 ± 0.4 Ma.
- (2) The granites in the Nianzigou Mo deposit are A-type and characterized by high SiO₂ and K₂O contents; enrichments in LILEs; marked depletions in Ba, Sr, P, and Ti; and small depletions in Ta and Nb. The granites have $10,000 \times \text{Ga/Al}$ ratios of 3.1–4.8 and show marked negative Eu anomalies.
- (3) Rhenium-Os isotopic dating of six molybdenite samples from the Nianzigou Mo deposit yielded model ages of 152.7–155.5 Ma (average = 153.9 Ma), which are similar to the zircon U-Pb ages of the host monzogranite and granite porphyry.
- (4) During the Late Jurassic period, northeast China began to transform from the Mongol–Okhotsk to the Paleo-Pacific tectonic regimes. The Nianzigou Mo deposit formed in a postorogenic extensional tectonic setting or during larger-scale lithospheric thinning during Early Yanshanian subduction of the Paleo-Pacific Plate beneath the NCC.

Supplementary Materials: The following are available online at <https://www.mdpi.com/article/10.3390/min12070791/s1>, Table S1: U-Pb isotopic dating result for zircons from the the Nianzigou granite, Table S2: trace-element (ppm) compositions of the Nianzigou granite, Table S3: Re-Os isotopic dating result for molybdenite from the Nianzigou granite, Table S4: major-element oxides (wt.%) of the Nianzigou granite.

Author Contributions: Conceptualization, Y.L. (Yang Li), Y.Y. and L.H.; methodology, Y.L. (Yaxing Leng); software, J.X.; supervision and project administration, Y.Y.; funding acquisition, Y.Y. All authors have read and agreed to the published version of the manuscript.

Funding: This research was supported by the National Natural Science Foundation of China (Grants 41272110) and the China Geological Survey Programs (12120114076801 and 12120113088900).

Data Availability Statement: Not applicable.

Acknowledgments: We thank Jiong-fei Zhang (chief engineer of geology) for his field discussion and Kylie Christiansen (Expert of Stallard Scientific Editing, New Zealand) for polishing the manuscript. We would also like to thank three anonymous reviewers for their constructive and thoughtful comments that have been helpful in improving the paper.

Conflicts of Interest: The authors declare no conflict of interest.

References

1. Groves, D.I.; Santosh, M. Craton and thick lithosphere margins: The sites of giant mineral deposits and mineral provinces. *Gondwana Res.* **2021**, *100*, 195–222. [[CrossRef](#)]
2. Kelley, K.D.; Huston, D.L.; Peter, J.M. Toward an effective global green economy: The Critical Minerals Mapping Initiative (CMMI). *SGA News* **2021**, *8*, 1–5.
3. Hoggard, M.J.; Czarnota, K.; Richards, F.D.; Huston, D.L.; Jaques, A.L.; Ghelichkhan, S. Global distribution of sediment-hosted metals controlled by craton edge stability. *Nat. Geosci.* **2019**, *13*, 504–510. [[CrossRef](#)]
4. Bars, A.; Miao, L.C.; Fochin, Z.; Baatar, M.; Anaad, C.; Togtokh, K.; Liu, Y. Petrogenesis and tectonic implication of the Late Mesozoic volcanic rocks in East Mongolia. *Geol. J.* **2018**, *53*, 2449–2470. [[CrossRef](#)]
5. Mao, J.W.; Wang, Y.T.; Zhang, Z.H.; Yu, J.J.; Niu, B.G. Geodynamic settings of Mesozoic large-scale mineralization in North China adjacent areas. *Sci. China Ser. D* **2003**, *46*, 838–851. [[CrossRef](#)]
6. Mao, J.W.; Xie, G.Q.; Zhang, Z.H.; Li, X.F.; Wang, Y.T.; Zhang, C.Q.; Li, Y.F. Mesozoic large-scale metallogenic pluses in North China corresponding geodynamic settings. *Acta Petrol. Sin.* **2005**, *21*, 169–188. (In Chinese with English abstract)
7. Liu, J.M.; Zhao, Y.; Sun, Y.L.; Li, D.P.; Liu, J.; Chen, B.L. Recognition of the latest Permian to Early Triassic Cu-Mo mineralization on the northern margin of the North China block and its geological significance. *Gondwana Res.* **2010**, *17*, 125–134. [[CrossRef](#)]
8. Dai, J.Z.; Mao, J.W.; Yang, F.Q. Geological characteristics and geodynamic background of Molybdenum (copper) deposits Along Yanshan-Liaoning metallogenic belt on Northern margin of North China Block. *Acta Petrol. Sin.* **2006**, *24*, 879–889. (In Chinese with English abstract)
9. Zhu, L.M.; Zhang, G.W.; Li, G.; Guo, B.; Yao, A.P.; Gong, H.J. Some key metallogenetic events of Qinling orogenic belt and their deposit examples. *J. NWU* **2009**, 381–391. (In Chinese with English abstract)
10. Shu, Q.H.; Lai, Y.; Zhou, Y.T.; Xu, J.J.; Wu, H.Y. Zircon U-Pb geochronology and Sr-Nd-Pb-Hf isotopic constraints on the timing and origin of Mesozoic granitoids hosting the Mo deposits in northern Xilamulun district, NE China. *Lithos* **2015**, *238*, 64–75. [[CrossRef](#)]

11. Zeng, Q.D.; Liu, J.M.; Chu, S.X.; Wang, Y.B.; Sun, Y.; Duan, X.X.; Zhou, L.L.; Qu, W.J. Re-Os and U-Pb geochronology of the Duobaoshan porphyry Cu-Mo-(Au) deposit, northeast China, and its geological Significance. *J. Asian Earth Sci.* **2014**, *79*, 895–909. [[CrossRef](#)]
12. Nie, F.J.; Zhang, W.Y.; Du, A.; Jiang, S.H.; Liu, Y. Re-Os isotopic dating on molybdenite separates from the Xiaodonggou porphyry Mo deposit, Hexigten Qi, Mongolia. *Acta Geol. Sin.* **2007**, *81*, 898–905.
13. Wu, H.Y.; Zhang, L.C.; Wan, B. Geochemistries, tectonic setting and mineralization potentiality of the ore-bearing monzogranite in the Kulitu molybdenum (copper) deposit of Xar moron metallogenic belt, Inner Mongolia. *Acta Petrolog. Sin.* **2008**, *24*, 867–878. (In Chinese with English abstract)
14. Chen, Y.J.; Zhang, C.; Li, N.; Yang, Y.F.; Deng, K. Geology of the Mo deposits in Northeast China. *J. Jilin Univ.* **2012**, *42*, 1223–1268. (In Chinese with English abstract)
15. Guo, F.; Fan, W.; Gao, X.; Li, C.; Miao, L.; Zhao, L. Sr-Nd-Pb isotope mapping of Mesozoic igneous rocks in NE China: Constraints on tectonic framework and Phanerozoic crustal growth. *Lithos* **2010**, *120*, 563–578. [[CrossRef](#)]
16. Chen, Z.G.; Zhang, L.C.; Wu, H.Y.; Wan, B.; Zeng, Q.D. Geochemistry study and tectonic background of A style host granite in Nianzigou molybdenum deposit in Xilamulun molybdenum metallogenic belt, Inner Mongolia. *Acta Petrolog. Sini.* **2008**, *24*, 879–889. (In Chinese with English abstract)
17. Zhai, D.G.; Liu, J.J.; Wang, J.P.; Yang, Y.Q.; Zhang, H.Y.; Wang, X.L.; Zhang, Q.B.; Wang, G.W.; Liu, Z.J. Zircon U-Pb and molybdenite Re-Os geochronology, and whole-rock geochemistry of the Hashitu molybdenum deposit and host granitoids, Inner Mongolia, NE China. *Asian Earth Sci.* **2014**, *79*, 144–160. [[CrossRef](#)]
18. Gao, S.; Chen, W.F.; Ling, H.F.; Sun, L.Q.; Ren, Q.; Xie, G.A.; Wang, K.X.; Tian, R.S. A latest Jurassic A-type granite in the Middle of Inner Mongolia: Petrogenesis and tectonic implications. *Lithos* **2021**, *394*, 106167. [[CrossRef](#)]
19. Yang, Y.Q.; Wu, L.W.; He, H.G. Origin of the Naoniushan Cu–Au deposit in Inner Mongolia, NE China: Constraints from fluid inclusions and H–O–S–Pb isotopes. *Geol. J.* **2020**, *55*, 5953–5966. [[CrossRef](#)]
20. Pearce, J. Sources and settings of granitic rocks. *Episodes* **1996**, *19*, 120–125. [[CrossRef](#)]
21. Loiselle, M.C.; Wones, D.R. Characteristics and origin of an orogenic granites. In Proceedings of the Annual Meetings of the Geological Society of America and Associated Societies, San Diego, CA, USA, 5–8 November 1979; Volume 11, p. 468.
22. Whalen, J.B.; Currie, K.L.; Chappell, B.W. A-type granites: Geochemical characteristics, discrimination and petrogenesis. *Contrib. Mineral. Petrol.* **1987**, *95*, 407–419. [[CrossRef](#)]
23. Bonin, B. A-type granites and related rocks: Evolution of a concept, problems and prospects. *Lithos* **2007**, *97*, 1–29. [[CrossRef](#)]
24. Ding, C.; Dai, P.; Bagas, L.; Nie, F.; Jiang, S.; Wei, J.; Ding, C.; Zuo, P.; Zhang, K. Geochemistry and Sr-Nd-Pb isotopes of the granites from the Hashitu Mo deposit of Inner Mongolia, China: Constraints on their origin and tectonic setting. *Acta Geol. Sin. Engl.* **2016**, *90*, 106–120.
25. Hu, X.L.; Yao, S.Z.; He, M.C.; Ding, Z.J.; Chen, B. Geochemistry, U-Pb geochronology and Sr-Nd-Hf isotopes of the Early Cretaceous volcanic rocks in the northern Da Hinggan Mountains. *Acta Geol. Sin. Engl.* **2015**, *89*, 203–216.
26. Zhai, D.G.; Liu, J.J.; Tombros, S.; Williams-Jones, A.E. The genesis of the Hashitu porphyry molybdenum deposit, Inner Mongolia, NE China: Constraints from mineralogical, fluid inclusion, and multiple isotope (H, O, S, Mo, Pb) studies. *Miner. Depos.* **2018**, *53*, 377–397. [[CrossRef](#)]
27. Chen, Y.J.; Zhang, C.; Wang, P.; Pirajno, F.; Li, N. The Mo deposits of Northeast China: A powerful indicator of tectonic settings and associated evolutionary trends. *Ore Geol. Rev.* **2017**, *81*, 602–640. [[CrossRef](#)]
28. Guo, X.G.; Li, J.W.; Zhang, D.H.; Xue, F.; Xian, H.B.; Wang, S.J.; Jiao, T.L. Petrogenesis and tectonic setting of igneous rocks from the Dongbulage porphyry Mo deposit, Great Hinggan Range, NE China: Constraints from geology, geochronology, and isotope geochemistry. *Ore Geol. Rev.* **2020**, *120*, 103326. [[CrossRef](#)]
29. Liu, W.; Yang, J.H.; Li, C.H. Thermochronology of three major faults in the Chifeng area, Inner Mongolia of China. *Acta Petrolog. Sin.* **2003**, *19*, 717–728. (In Chinese with English abstract)
30. Zhai, D.G.; Williams-Jones, A.E.; Liu, J.J.; Selby, D.; Voudouris, P.C.; Tombros, S.; Li, K.; Li, P.L.; Sun, H.J. The genesis of the Giant Shuangjianzishan Epithermal Ag Pb-Zn deposit, Inner Mongolia, Northeastern China. *Econ. Geol.* **2020**, *115*, 101–128. [[CrossRef](#)]
31. Wu, F.Y.; Sun, D.Y.; Ge, W.C.; Zhang, Y.B.; Grant, M.L.; Wilde, S.A.; Jahn, B.M. Geochronology of the Phanerozoic granitoids in northeastern China. *J. Asian Earth Sci.* **2011**, *41*, 1–30. [[CrossRef](#)]
32. Zhang, L.C.; Wu, H.Y.; Wan, B.; Chen, Z.G. Ages geodynamic settings of Xilamulun Mo–Cu metallogenic belt in the northern part of the North China Craton. *Gondwana Res.* **2009**, *16*, 243–254. [[CrossRef](#)]
33. Wu, H.Y.; Zhang, L.C.; Pirajno, F.; Xiang, P.; Wan, B.; Chen, Z.G.; Zhang, X.J. The Jiguanshan porphyry Mo deposit in the Xilamulun metallogenic belt, northern margin of the North China Craton, U-Pb geochronology, isotope systematics, geochemistry and fluid inclusion studies: Implications for a genetic model. *Ore Geol. Rev.* **2014**, *56*, 549–565. [[CrossRef](#)]
34. Eggins, S.M.; Kinsley, L.P.J.; Shelley, J.M.M. Deposition elemental fractionation processes during atmospheric pressure laser sampling for analysis by ICP-MS. *Appl. Surf. Sci.* **1998**, *127*, 278–286. [[CrossRef](#)]
35. Jackson, S.E.; Pearson, N.J.; Griffin, W.L.; Belousova, E.A. The application of laser ablation-inductively coupled plasma–mass spectrometry to in situ U-Pb zircon geochronology. *Chem. Geol.* **2004**, *211*, 47–69. [[CrossRef](#)]
36. Andersen, T. Correction of common lead in U-Pb analyses that do not report ²⁰⁴Pb. *Chem. Geol.* **2002**, *192*, 59–79. [[CrossRef](#)]
37. Ludwig, K.R. *ISOPLOT 3.00: A Geochronological Toolkit for Microsoft Excel*; Berkeley Geochronology Center: Berkeley, CA, USA, 2003.

38. Du, A.D.; Wu, S.Q.; Sun, D.Z.; Wang, S.X.; Qu, W.J.; Markey, R.; Stein, H.; Morgan, J.; Malinovsky, D. Preparation and certification of Re-Os dating reference materials, molybdenite HLP and JDC. *Geostand. Geoanal. Res.* **2004**, *28*, 41–52. [[CrossRef](#)]
39. Hoskin, P.W.O. Trace-element composition of hydrothermal zircon and the alteration of Hadean zircon from the Jack Hills, Australia. *Geochim. Cosmochim. Acta* **2005**, *69*, 637–648. [[CrossRef](#)]
40. Sun, S.S.; McDonough, W.F. Chemical and isotopic systematics of oceanic basalts: Implications for mantle composition and processes. In *Magmatism in Ocean Basins*; Saunders, A.D., Norry, M.J., Eds.; Geological Society of Special Publication: London, UK, 1989; Volume 42, pp. 313–345.
41. Middlemost, A.K. Naming materials in the magma/igneous rock system. *Earth Sci. Rev.* **1994**, *37*, 215–224. [[CrossRef](#)]
42. Pearce, J.A.; Harris, N.B.W.; Tindle, A.G. Trace element discrimination diagrams for the tectonic interpretation of granitic rocks. *J. Petrol.* **1984**, *25*, 956–983. [[CrossRef](#)]
43. Peccerillo, R.; Taylor, S.R. Geochemistry of Eocene calc-alkaline volcanic rocks from the Kastamonu area, northern Turkey. *Contrib. Mineral. Petrol.* **1976**, *50*, 63–81. [[CrossRef](#)]
44. Frost, B.R.; Frost, C.D. A Geochemical Classification for Feldspathic Igneous Rocks. *J. Petrol.* **2008**, *49*, 1955–1969. [[CrossRef](#)]
45. Papoutsas, A.; Pe-Piper, G.; Piper, D.J.W. Systematic mineralogical diversity in A-type granitic intrusions: Control of magmatic source and geological processes. *Geol. Soc. Am. Bull.* **2016**, *128*, 487–501. [[CrossRef](#)]
46. Condamine, P.; Médard, E. Experimental melting of phlogopite-bearing mantle at 1GPa: Implications for potassic magmatism. *Earth Planet. Sci. Lett.* **2014**, *397*, 80–92. [[CrossRef](#)]
47. Landenberger, B.; Collins, W.J. Derivation of A-type Granites from a Dehydrated Charnockitic Lower Crust: Evidence from the Chaelundi Complex, Eastern Australia. *J. Petrol.* **1996**, *37*, 145–170. [[CrossRef](#)]
48. Zhao, X.F.; Zhou, M.F.; Li, J.W.; Wu, F.Y. Association of Neoproterozoic A- and I-type granites in South China: Implications for generation of A-type granites in a subduction-related environment. *Chem. Geol.* **2008**, *257*, 1–15. [[CrossRef](#)]
49. Patiño Douce, A.E. Generation of metaluminous A-type granites by low-pressure melting of calc-alkaline granitoids. *Geology* **1997**, *25*, 743–746. [[CrossRef](#)]
50. Huang, H.Q.; Li, X.H.; Li, W.X.; Li, Z.X. Formation of high $\delta^{18}\text{O}$ fayalite-bearing A-type granite by high temperature melting of granulitic metasedimentary rocks, southern China. *Geology* **2011**, *39*, 903–906. [[CrossRef](#)]
51. Creaser, R.A.; Price, R.C.; Wormald, R.J. A-type granites revisited: Assessment of a residual-source model. *Geology* **1991**, *19*, 163–166. [[CrossRef](#)]
52. Miller, C.F.; McDowell, S.M.; Mapes, R.W. Hot and cold granites? Implications of zircon saturation temperatures and preservation of inheritance. *Geology* **2003**, *31*, 529. [[CrossRef](#)]
53. Dall’Agnol, R.; de Oliveira, D.C. Oxidized, magnetite-series, rapakivi-type granites of Carajás, Brazil: Implications for classification and petrogenesis of A-type granites. *Lithos* **2007**, *93*, 215–233. [[CrossRef](#)]
54. Ji, Z.; Meng, Q.A.; Wan, C.B.; Zhu, D.F.; Ge, W.C.; Zhang, Y.L.; Yang, H.; Dong, Y. Geodynamic Evolution of Flat-Slab Subduction of Paleo-Pacific Plate: Constraints from Jurassic Adakitic Lavas in the Hailar Basin, NE China. *Tectonics* **2019**, *38*, 4301–4319. [[CrossRef](#)]
55. Liu, H.T.; Zhai, M.G.; Liu, J.M.; Sun, S.H. The Mesozoic granitoids in the northern marginal region of North China Craton: Evolution from post-collisional to anorogenic settings. *Acta Petrol. Sin.* **2002**, *18*, 433–448.
56. Lin, Q.; Ge, W.C.; Wu, F.Y.; Sun, D.Y.; Cao, L. Geochemistry of Mesozoic granitoids in Da Hinggan Mountains Range. *Acta Petrol. Sin.* **2004**, *20*, 403–412.